Oecologia (1996) 108:1–12

Robert W. Pearcy · Weimin Yang

A three-dimensional crown architecture model for assessment of light capture and carbon gain by understory plants

Received: 11 September 1995 / Accepted: 5 March 1996

Abstract A model simulating the three-dimensional crown architecture of a plant was developed with the objective of assessing the light capture and whole-plant carbon gain consequences of leaf display in understory plants. This model uses geometrical measurements taken in the field to reconstruct the projected image of a plant so that light absorption from any direction can be assessed. The photon flux density (PFD) from a given direction was estimated from the canopy openness derived from hemispherical canopy photographs and equations simulating the daily course of direct and diffuse PFD. For diffuse PFD, the directional fluxes and absorbed PFD were integrated over 160 different directions representing 8 azimuth classes and 20 elevation angle classes. Direct PFD absorption was determined for the time that a solar track on a given day intersected a canopy gap. Assimilation rate was simulated for the sunlit and shaded parts of leaves separately and then summed to give the whole-plant carbon gain. Comparisons of simulations for a tropical forest edge species, *Clidemia octona*, and an understory species, *Conostegia cinnamomea*, illustrate the operation of the model and show that the edge species is more efficient at capturing side light while the understory species is slightly more efficient at capturing light from directly above, the predominant light direction in this environment. Self-shading within *Conostegia* crown and steep leaf angles in the *Clidemia* crown reduced light capture efficiencies for light from directly above. Whole-plant daily carbon gain was much higher in the forest edge site, mostly because of the additional PFD available in this site. However, simulations for both species in the understory light environment show that the higher light capture efficiencies of the understory species in this environment conferred a 27% advantage in carbon gain in this environment.

R.W. Pearcy (✉) · W. Yang
Section of Plant Biology,
University of California,
Davis, CA 95616, USA
fax: 916-752-5410,
e-mail: rwpearcy@ucdavis.edu

Key words Crown architecture · Carbon gain · Light capture · Understory plants

Introduction

The arrangement of leaves within the crown of a plant influences many aspects of whole-plant function including photosynthesis, transpiration and energy balance. In shaded environments the optimal form is assumed to be an arrangement which minimizes leaf overlap and in which the leaf surfaces are perpendicular to the light source. In high light environments, increased leaf angles, especially near the crown periphery, and multilayer crowns are assumed to provide an advantage by distributing the available photon flux density (PFD) at optimal levels over all leaves. Real plants in sun and shade environments may deviate considerably from these patterns because of various constraints on crown form, including for example the biomechanical cost of support (Chazdon 1986; Givnish 1986) and the interactions between branches resulting from the modular nature of plants. Moreover, real plants are a product of their past environment, which may leave them developmentally constrained with respect to optimal crown form for the current environment if it has changed significantly.

The understanding of the role of crown architectural characteristics in light capture has relied extensively on both qualitative and quantitative models. Models of homogeneous continuous canopies of forests or crops have been used to provide insight into the role of specific characteristics such as leaf angle and leaf area index or the vertical distribution of leaf characteristics such as leaf mass per unit area or leaf N (Monsi et al. 1973; Gutschick and Weigel 1988). For individual plants such as trees, qualitative models of branching have been used to describe the development of form (Halle et al. 1978) but these have had limited ecological applicability in understanding how specific architectures influence resource capture. Two-dimensional models have been used to explore how branch angle and branch length influence leaf

overlap and hence the efficiency of light capture (Fisher and Honda 1977a, b; Honda and Fisher 1978; Fisher 1986). Similarly, the projected area of understory palm canopies has been used to assess the efficiency of whole-plant light interception (Chazdon 1985). These approaches are limited in that they consider the interception of light from only a single direction, whereas, in reality, diffuse PFD comes from many directions and the direction of the solar beam changes during the day. Recently, three-dimensional models have been used to assess light interception by individual plants or shoots. These models have generally been focused on either relatively simple shoot structures representing specific phyllotactic patterns (Niklas 1988), or are species-specific (Dickmann et al. 1990), or have considered the crown as a series of layers, shells or cells with particular foliage characteristics in each (Myneni and Impens 1985; Wang and Jarvis 1990; Whitehead et al. 1990; Ryel et al. 1993). Myneni (1991) has used fractal models of trees to simulate leaf area distributions for modelling radiative transfer and photosynthesis in a forest canopy.

In this paper we present a three-dimensional crown architecture model, suitable for assessing the light capture and photosynthesis of small plants under specific canopy conditions. The model, which we have named YPLANT, reconstructs a plant in three-dimensional space from geometric measurements recorded for each element (stem segment, branch segment, leaf) in the crown of a plant in order to assess the consequences of crown architecture on light capture. Since the total light capture depends on allocation of biomass to leaf area (the leaf area ratio) and the efficiency with which this leaf area is displayed, we developed a complementary allometric approach to estimate biomass and allocation parameters from the same data set. A simple photosynthesis submodel allows computation of whole-plant carbon gain. For understory plants, hemispherical canopy photographs analyzed with the program CANOPY (Rich 1990) are used to determine the directional components of both diffuse and direct solar radiation so that the specific relationship between crown architecture and the light environment can be simulated. We describe the structure of YPLANT and then present an example of its utility in assessing light capture by individual plants.

Material and methods

The model

YPLANT was written in Borland Pascal and runs on an IBM-compatable PC computer with at least an 80386 processor and preferably a color monitor. The program is available for use by others and can be obtained upon request from the authors. It makes extensive use of graphical images for both visualization of crown morphology and analysis of the consequences of this morphology. Input for the model is from geometric measurements made on plants in the field, physiological measurements of leaf gas exchange properties, and from data derived from canopy gap distributions recorded by hemispherical canopy photographs. The latter was obtained using an image analysis program (CANOPY) specifically developed for this purpose. Below we briefly describe the structure of the model and the input parameters required for its operation.

Simulation of the three-dimensional crown architecture

The computer reconstruction of crown architecture was based on the "node" as the fundamental unit with a plant consisting of a series of articulated nodes, each connected and supported by a "stem" segment. We use the term stem segment here to refer to either a length of stem or a branch originating at a node and extending to the next node. We chose the simplest case of each node potentially having a stem, a branch and a leaf connected to the node by a petiole, although at any given node any or all of these components could be missing. More complex architectures such as opposite or whorled leaves can be simulated by assuming multiple nodes with a vanishingly small (0.1 mm) stem length between them. Thus, in effect, for opposite leaves, two nodes, each with a leaf, were simulated at essentially the same point in space. Obviously, no necessary correspondence existed between true nodes and model nodes. If true nodes along a straight stem segment lacked leaves or branches, they added no particular information to the model and therefore were not recorded. Assignment of a particular stem segment as being either a "branch" or a "stem" from the node was arbitrary and not based on any developmental principles. Its primary function was to determine the path between two connected nodes. For each node, the node of origin (the "mother" node) and whether it is connected via the stem or branch to that mother node was recorded.

Each stem segment was described by its length, l, diameter, d, and elevation angle, α, measured from the horizontal, and azimuth, β, measured in the proximal to distal direction (Fig. 1). Internodes were assumed to be cylinders of uniform diameter given by d, surrounding the central axis connecting the proximal and

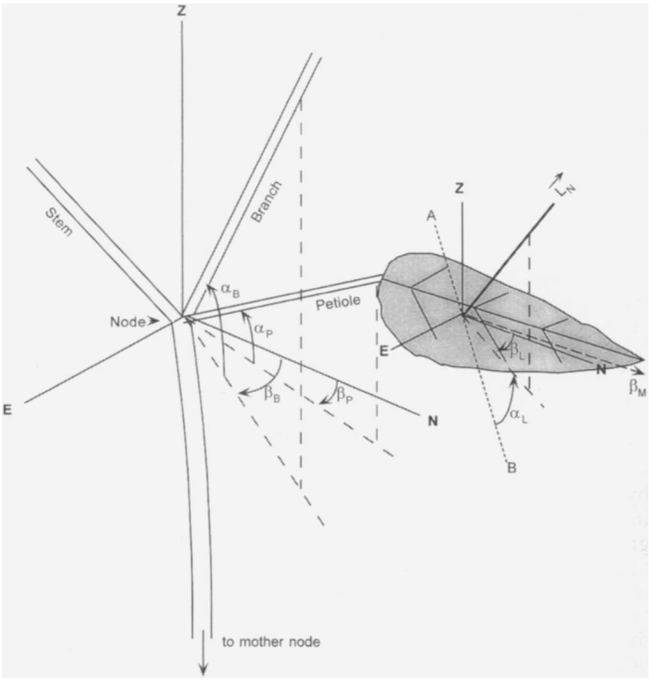

Fig. 1 Diagram showing angles (α), azimuths (β) specifying the architecture of a plant at a node. $\bar{L}_N$ is the vector normal to the leaf surface while the line *A–B* is the steepest surface on the leaf. The angle and azimuth defining the stem position and the relevant lengths and diameters that are also required by YPLANT are omitted for clarity. See the text for details

distal nodes. The same measurement system was applied to petioles where the distal end was the petiole attachment point of the leaf.

Leaf geometry, independent of leaf size, was simulated from its surface orientation, and a set of coordinates describing the shape of the leaf (see Appendix 1). All leaves were treated for simplicity as planar surfaces, i.e. with no curvature. Coordinates for the leaf edge were determined by tracing the leaf onto graph paper and assigning the coordinates $x = 0$, $y = 0$ to the petiole attachment point and the y axis to the longitudinal axis of the leaf. Up to 40 points were used to describe the shape, though most leaves could be adequately described by <25 points. These relative coordinates were then scaled to absolute coordinates based on the measured leaf length to give the correct leaf size. Thus, different-sized leaves of the same general shape could be accommodated with only one set of leaf-edge coordinates. Leaves of different shapes were accommodated by allowing for up to 20 different leaf types in the simulation, with each type having its own set of leaf-edge coordinates. The angle (α_l) and azimuth (β_l) of the leaf surface was taken as the angle to the horizontal of the steepest slope of the surface and the azimuth of the normal to this surface, respectively. The azimuth of the leaf longitudinal axis (β_m), which usually corresponded to the midrib azimuth, was also recorded, as it was a necessary parameter for proper orientation of the leaf in three-dimensional space.

Estimation of the absorption cross section of a crown

We define the absorption cross section of a crown as the displayed area times the absorptance. To estimate the absorption cross section, a projected image of the crown in a plane perpendicular to the beam must be derived. For this purpose, two coordinate systems were used to simulate the geometric projection of the plant in three-dimensional space. The first, the "Earth" coordinate system, is given by the e, n and z-axis system corresponding to East, North, and the zenith directions, respectively. Plant measurements, the canopy photograph and the geometric description of the solar track all utilized this coordinate system. Vectors to each node were calculated, based on the vector to the mother node and the vector of the stem segment (see Appendix 1). Vectors to the petiole attachment point of the leaf were determined in a similar manner. Vectors were then calculated to the leaf-edge coordinates so that the leaves were arrayed in their proper orientations.

A second coordinate system was then used to project the image onto the plane. This "viewpoint" coordinate system was given by a x, y and v axis with the v axis always being normal to the monitor screen. Within the Earth coordinate system, the v axis was always antiparallel to the light vector and the x axis was always parallel to the Earth's surface and pointed to the right. Therefore, the image consisted of a parallel projection of the crown as if it were being viewed from the vector of an incident light beam. The method of conversion from earth to viewpoint coordinates is given in Appendix 2. The apparent area of leaves visible in this direction is that modified by the cosine of the angle of incidence on the surface and by leaf overlap causing self-shading. The absorption cross section for each leaf on the plant in the x-y plane was determined by sampling a grid to determine the number of gridpoints falling inside the boundaries of a leaf using a ray-tracing procedure. The grid size was varied, depending on the particular plant geometry, to achieve a compromise between maximizing sampling accuracy and reasonable speed. If a gridpoint fell within the boundaries of two or more leaves then the relative positions of these leaves on the v-axis was calculated so that which leaves were shaded by the other or others could be determined. Gridpoint summations were made separately for the shaded and unshaded parts of a leaf, and for the shaded parts, the number of gridpoints in areas shaded by 1,2...n leaves. The fractions of the leaf that were unshaded (f_{USH}) and shaded (f_{SH}) with respect to PFD incident from a vector, **V**, or shaded by 1,2...n leaves were then determined as

$$f_{USH} = G_{USH}/G_{TOTAL}$$

and

$$f_{SH} = 1 - G_{USH}$$

where $G_{USH}$and G_{SH} are the number of gridpoints within the unshaded and shaded parts of the leaf, respectively. The absorbed photon power in μmol photons s^{-1} per gridpoint incident on a leaf n at gridpoint g ($P_{n,g}$) was given by:

$$P_{n,g} = a_n I_{P,n} d^2 \quad (1)$$

where a_n is the absorptance of leaf n, $I_{P,n}$ is the PFD at the leaf surface but perpendicular to the beam, which was normalized to a value of 1 for unshaded gridpoints, and d is distance between gridpoints. For shaded gridpoints, $I_{P,n}$ was the normalized PFD transmitted through the shading leaves as given by:

$$I_{P,n} = I_{P,(n+1)}(1-a_{(n+1)}-r_{(n+1)}) \quad (2)$$

where n refers to the successive leaves along the vector and a and r are the respective leaf absorptance and reflectance. Thus the second term on the right side of Eq. (2) reduces I_P on leaf n to the amount transmitted through leaf $n + 1$. Gridpoints shaded by stems or petioles were assumed to receive no PFD from that vector. The normalized absorbed PFD for leaf n were given by:

$$I = \frac{\sum_{i=1}^{g} P_{n,g}}{L_n} \quad (3)$$

where L_n is the leaf area. YPLANT calculated a relative area for a leaf shape as a fraction of a square with sides equal to the leaf length. Therefore the area of a leaf of length l could be calculated as this fraction times l^2. In the case of direct PFD, $P_{n,g}$ for the shaded and unshaded fractions of the leaf were summed separately and L in Eq. 3 was the respective shaded or unshaded leaf area. This procedure allowed for calculation of the assimilation rate of the shaded and unshaded portions separately.

Determination of absorbed PFD

Diffuse PFD. To estimate the actual PFD arriving at the plant from a particular sky sector, we first simulated the PFD on a plane normal to the solar beam above the overstory canopy (F_P) as a function of the maximum value above the atmosphere and an atmospheric transmission coefficient that varied with the pathlength through the atmosphere as:

$$F_P = F_M \tau_a^{\frac{1}{\sin\alpha}} \quad (4)$$

where F_M is the maximum PFD on a normal plane outside of the atmosphere (the solar constant for PFD), τ_a is the atmospheric transmission coefficient, and α_s is the solar elevation angle (Campbell 1977). We set τ_a equal to 0.84 to simulate a clear day (Campbell 1977). We set the normalized diffuse PFD (I_{DIF}) above the overstory canopy to be 0.1 of the normalized direct PFD (I_{DIR}), which is a reasonable approximation for measured values under clear skies. We considered the sky to be divided into 160 different sectors defined by 20 elevation angle (α) classes and 8 azimuth (β) classes, which were the same as those used in CANOPY (Rich 1990). To arrive at the necessary PFD flux from each sector to give 0.1 of the direct PFD, it was necessary to invert the functional relationship between the normalized PFD on a horizontal surface and the normalized PFD from any sky sector (I_i) such that

$$\sum_{i}^{160} I_i = 0.1\, I_{DIR} \quad (5)$$

Where I_i is the normalized PFD contributed from the ith sector. The area of any sector of the sky (Ω_s) is given by

$$\Omega_s = \int_{\beta_1}^{\beta_2}\int_{\alpha_1}^{\alpha_2} r^2 \sin\alpha d\alpha\, d\beta = r^2(\beta_2 - \beta_1)(\cos\alpha_1 - \cos\alpha_2) \quad (6)$$

Since $\beta_2 - \beta_1 = \frac{\pi}{4}$, then

$$\Omega_s = \frac{\pi r^2}{4}(\cos\alpha_1 - \cos\alpha_2) \quad (7)$$

Inversion of the diffuse PFD on a horizontal surface to the PFD from a sky sector is based on the relationship that if the photon flux from every part of the sky is equal to K, then the normalized PFD from a particular sky sector is:

$$I_s = \frac{K}{\Omega_s} \quad (8)$$

If a horizontal surface of unit area receives a normalized diffuse PFD equal to I_{DIF}, then

$$I_{\mathrm{DIF}} = \sum_i^{160} I_i \cdot \cos(\tilde{\alpha}_i) = \sum_i \frac{K}{\Omega_i} \cdot \cos(\tilde{\alpha}_i) = K \sum_i \frac{\cos(\tilde{\alpha}_i)}{\Omega_i} \quad (9)$$

where $\tilde{\alpha}_i$ is the elevation angle to the centroid of the sector. It follows that

$$K = \frac{I_{\mathrm{DIF}}}{\sum_i \frac{\cos(\tilde{\alpha}_i)}{\Omega_i}} \quad (10)$$

and

$$I_s = \frac{I_{\mathrm{DIF}}}{\sum_i \frac{\cos(\tilde{\alpha}_i)}{\Omega_i}\Omega_s} \quad (11)$$

Setting the denominator in Eq. 11 equal to S_{FS} gives

$$I_s = \frac{I_{\mathrm{DIF}}}{S_{\mathrm{FS}}} \quad (12)$$

The output from CANOPY contains indirect site factors (ISF) for each sector. ISF is defined as the fractional canopy openness in a sector times the relative contribution of that sector to the total hemispherical ISF. Since we assumed a uniform sky brightness distribution (UOC), the fractional canopy openness (o_s) was given by $\mathrm{ISF}_S \cdot 160$. The incident diffuse PFD ($I_{\mathrm{DIF},s}$) from any sector, s, reaching the plant crown was then calculated from the fraction of open sky (o_S) in sector s as:

$$I_{\mathrm{DIF},s} = \frac{0.1[o_s(1 - T_C) + T_C]}{S_{\mathrm{FS}}} \quad (13)$$

where T_C is an overstory canopy transmission coefficient. This equation accounted for attenuation of $I_{\mathrm{DIF},s}$ along the vector **V** by the overstory canopy as a function of its openness and canopy transmission coefficient. The T_C is the fractional transmission of the "closed" part of the canopy where the gaps between leaves were too small to be registered on the photographic image, and where transmission through leaves and reflected PFD still contributed to the diffuse PFD from the sector. In practice, we set T_C to give about 5 μmol photons m^{-2} s^{-1} at midday for a completely "closed" canopy ($T_C = 0.04$). The UOC has been shown to slightly underestimate diffuse radiation in the understory as compared to other theoretical distributions when applied to canopy photographs (Hutchison et al. 1980). This underestimation is offset by T_C, which increases the predicted diffuse PFD.

The PFD absorbed by leaf n from sector s was then calculated as

$$F_{\mathrm{DIF},s} = I_{\mathrm{DIF},s} \cdot F_P \quad (14)$$

Since $I_{\mathrm{DIF},s}$ depended on the architecture of the overstory canopy and the plant, but not the time of the day, it was possible to considerably speed the computations by calculating values of $I_{\mathrm{DIF},s}$ only once and storing them in an array. Then Eqs. 4 and 14 could be applied using these stored values. The absorbed diffuse PFD by leaf n was then calculated as:

$$F_{\mathrm{DIF}} = \frac{\sum_{s=1}^{160} F_{\mathrm{DIF},s}}{160} \quad (15)$$

Computation of the absorbed PFD were made at defined intervals during the day to take into account the diurnal variation in F_P and whenever there was also computation of direct PFD contributed by a sunfleck (see below). The sampling interval is set as an operational parameter in YPLANT but has a default value of 30 min.

Direct PFD. The absorption of direct beam PFD occurs when a gap in the canopy as recorded on the canopy photograph coincides with the solar track for a specific day. CANOPY determines the time along a specific solar track when a gap is intercepted, providing for each gap the start and stop time for the direct PFD (sunfleck or gap). Specific solar tracks are calculated from the date and latitude. We also made a provision in YPLANT for reading in a reduction factor, k, that could range from 0 to 1 and that reduced the predicted direct PFD in sunflecks to values more similar to those observed in the field as influenced by penumbral effects, etc. The model was run for a specific day and when the solar track intercepted a gap as indicated by the start and stop times, the model calculations were done for both diffuse PFD and for direct PFD for the vector defined by the solar azimuth and angle. For direct PFD periods shorter than the minimum sampling interval, the calculations were done at the midpoint of the interval and applied to the whole interval. For longer intervals, during which changes in solar coordinates would be important, the calculations were done 2 or more times, with each being applied for the respective part of the total direct light period.

The absorption of direct PFD was calculated in a manner analogous to that utilized for diffuse PFD absorption. The direct beam PFD was calculated from Eq. 4, while Eq. 2 was also applied to calculate the PFD on the shaded leaf parts. We applied Eq. 3 separately for the shaded and unshaded fractions by summing $P_{n,g}$ separately for each fraction using the respective leaf area for the shaded and unshaded fraction. The absorbed sunfleck PFD at time t ($F_{\mathrm{DIR},t}$) was then calculated as:

$$F_{\mathrm{DIR},t} = I_{\mathrm{DIR},t} \cdot k \cdot F_{P,t} \quad (16)$$

Where $F_{P,t}$ is the normal direct beam PFD at time t.

As an alternative to deriving sunfleck records from fisheye photographs, we also developed a procedure for deriving the start and stop times for sunflecks and k from direct measurements of PFD over the plant. The PFD was measured with GaAsP photocells (Hanamatsu, model G1118) and recorded at 1-s intervals with a portable datalogger (Campbell Scientific, model CR21X). A program, HISTO, was then used to determine the occurrence of a sunfleck in the record based on the time that the PFD exceeded a threshold value. HISTO recorded the start time, sunfleck duration, and the integrated total and maximum PFD of the sunfleck. To simplify the record, sunflecks occurring within 15 min were merged into one, and the duration calculated to give the same integrated PFD as the total for all merged sunflecks when k = 0.6. This value of k was used since sunflecks, or, in particular, clusters of sunflecks, often exhibited a more or less distinct rise and fall analogous to one-half of a sine wave. A value of 0.6 therefore gave a reasonable estimate of the mean maximum PFD in the cluster. Sunfleck records created in this way were appended to the CANOPY output file so they could be processed by YPLANT.

Efficiency of light capture

YPLANT calculated the efficiency of light capture (E_A) as the ratio of the mean PFD absorbed by the crown to the PFD incident on a horizontal surface. A horizontal surface served as the standard

since this is the plane in which PFD measurements are usually taken. The E_A calculated in this way takes into account the effects of leaf angle and leaf overlap on light interception as well as the effects of leaf absorptance, transmittance and recapture by lower leaves. Since both the absorbed and incident PFDs are derived from the canopy photograph analysis, E_A is not influenced by inaccuracies in predicting the actual PFD level. In previous crown architecture studies, light interception efficiencies (E_I) rather than absorption efficiencies have typically been determined. If leaf absorptance is set to 1, then $E_A = E_I$. YPLANT also calculates and stores in a file the projected leaf area (L_P) and displayed leaf area (L_D) for each sky sector in the diffuse light determinations and for each sample time along the solar track. L_P is the effective area of all leaves in the viewpoint plane without leaf overlap whereas L_D includes the effects of leaf overlap (self shading). Projection (E_P) and display (E_D) efficiencies, which provide a quantitative indication of the roles of leaf orientation and self shading in light capture efficiency of a crown, were calculated as $E_P = L_P / L_T$ and $ED = L_D / L_T$ where L_T is the total leaf area.

If the biomass (M) of the plant is known (see methods) then a light absorption efficiency per unit of biomass can be calculated from the output of YPLANT in a manner analogous to that for E_A. If F_T is the PFD absorbed by the plant, then the PFD captured per unit of biomass (F_M) is obtained as

$$F_M = \frac{F_T \cdot L_T}{M} \tag{17}$$

and has the units μmol photons g^{-1} s^{-1}. It therefore follows that the ratio of F_M to the incident PFD on a horizontal surface has the units of m^2 g^{-1}. We term this ratio the effective leaf area ratio, (LAR_E) since it has the same units as LAR but quantifies how the efficiency of this LAR is reduced by architectural constraints within the crown. LAR_E can also be calculated from E_A and the LAR determined from M and the total leaf area as $LAR_E = E_A \cdot LAR$. The effective leaf area ratio gives a quantitative measure of the effect of crown architecture on the efficiency of deployment of biomass in leaves for light capture. It therefore has an advantage over leaf-area based measures such E_A in that it includes the effects of both biomass allocation and of the architectural display of the leaves on whole-plant light capture.

Simulation of assimilation rate

The assimilation rate of each leaf type was modeled using the rectangular hyperbolic response to PFD:

$$A_N(I) = \frac{(\phi aI + (A_{MAX} + R)) - \sqrt{(aI + A_{MAX} + R)^2 - 4\theta aI(A_{MAX} + R)}}{2\theta} - R \tag{18}$$

where A_N is the net photosynthetic rate at the absorbed PFD, F, where $F = F_{DIR} + F_{DIF}$, A_{MAX} is the light-saturated net photosynthetic rate, R is the respiration rate in the dark, ϕ is the quantum yield for CO_2 assimilation, and θ is the convexity of the curve, which ranges from 0 to 1 for gradual to abrupt transitions from light limitation to saturation (Thornley 1976). The appropriate parameter values were determined from measured light-response curves by a least-squares fit to the model using the non-linear regression routines in SigmaPlot (Jandel Scientific). YPLANT calculated A_N for the shaded and unshaded portions of the leaf separately.

Operation of the model

The architectural data for a given plant were stored in a "plant" file following a defined format. These files were created with a spreadsheet and contained all the plant-specific information required to define the position of the stems and leaves in space, the appropriate leaf type at each node, and the absolute size (length) of the leaf. A second file (the "leaf" file) was also created with a spreadsheet and contained the leaf edge coordinates, A_{MAX}, R, ϕ, θ, a and T for each leaf type. A canopy file, if one had been created, contained the output from CANOPY, including the diffuse site factors and the times of direct PFD during the day. The model was run by first specifying leaf and plant files and, if desired, a canopy file. If no canopy file was specified, the calculations could be performed for a completely open sky, in which case a default canopy file containing diffuse site factors for an open sky was used. The normalized diffuse PFD absorption was then determined and stored in an array. The date and latitude were then specified so that calculations for the direct PFD for a specific solar track could then be made. Individual leaves could also be selected for output of leaf-specific light absorption and assimilation rates, which were useful in analyzing effects of position within the canopy, or the consequences of different physiological parameters. In addition, the L_P and L_D for each selected leaf was output. Up to 20 leaves in a given simulation could be selected for this leaf-by-leaf analysis.

The simulation was then run, during which the plant was displayed in the viewplane at each point where a calculation of direct PFD absorption was made. The output from the model at each sample time consisted of:

1. The simulated PFDs on horizontal surfaces above and below the overstory canopy as recorded by the canopy photograph.
2. The mean direct, diffuse and total PFD absorbed by the plant. The direct PFD was also reported as the amounts absorbed by the sunlit and by the self-shaded fractions of the crown.
3. The efficiency of light absorption (E_A).
4. The mean assimilation rate for the sunlit and self-shaded fractions of the crown and the overall mean rate.
5 The apparent photon efficiencies for CO_2 assimilation calculated on an incident (horizontal surface) and an absorbed light basis.
6. The daily totals of absorbed PFD and assimilation.

Output for the diffuse light simulation consisted of:

1. The L_P and L_D of the whole plant for each sky sector.
2. The L_P and L_D of the selected leaves for each sky sector.

In addition, for each selected leaf and each time during the day the output consisted of:

1. The L_P and L_D for the vector defined by the azimuth and elevation angle of the sun.
2. The absorbed PFD.
3. The assimilation rate.

The outputs were saved in files which could be read into a spreadsheet program for further analysis.

Methods

Measurements were made on two shrubs from the family Mellestomataceae occurring at the Smithsonian Tropical Research Institute Barro Colorado Island Field Station in March 1995. *Conostegia cinnamomea* is typically 1–2 m tall and is common in the forest understory. *Clidemia octona* is a 2- to 3-m-tall-shrub found at the forest edge. The *Conostegia* individual selected for measurement was located adjacent to T. Barbour trail about 200 m from the laboratory clearing while the *Clidemia* individual measured was at the edge of the laboratory clearing. Leaf angles were measured with a protractor mounted on a plastic bar with a bubble level attached. The edge of the protractor was adjusted to be parallel to the steepest leaf surface when the bar was held horizontal. A compass mounted on the bar allowed the leaf azimuth to be read in the same operation. Leaf orientation was measured by aligning the bar with the longitudinal axis of the leaf and reading the compass direction. Angles and azimuths of stem segments and petioles were measured in a manner analogous to those for leaves. Lengths and diameters were measured with a ruler and calipers, respectively. An outline of a representative leaf was traced onto graph paper to determine the coordinates for the leaf shape.

To determine the biomass of each plant, we harvested branches and leaves of nearby individuals and then constructed allometric

relationships between stem diameter and dry mass and petiole diameter and dry mass. Dry masses were determined after oven drying at 60°C for 36 h. Measurements of leaf area with a leaf area meter (LI-COR, model 3100) and leaf dry mass were used to determine leaf mass per unit area (LMA). These relationships were then applied to the stem and petiole length and diameter data in the YPLANT file to calculate masses. Total leaf mass was determined from the area given by YPLANT and the LMA.

Hemispherical (fisheye) canopy photographs were taken at the top of the crown of each plant using an 8 mm Nikkor fisheye lens mounted on a Nikon camera. The internal red filter in this lens was used to increase contrast. Kodak Tri-X film was used. Photographs were taken on clear days just before sunset afternoon when reflections of direct light from leaves was not a problem. The resulting images were analyzed using a Nikon 55 mm micro lens mounted on Cohu model 4815 video camera attached to a Data Translation Model 2853 frame grabber board in a 386 PC computer. The program CANOPY (Rich 1990) was used to determine the distribution of gaps for both diffuse and direct light penetration to the target plant as discussed above.

The daily course of incident PFD was measured with Hanamatsu model G1118 GaAsP photocells connected to a Campbell Scientific model CR21X datalogger. For each shrub, a total of 6 sensors supported by wooden dowels at the top of the crown were used, with logging of the PFDs occurring at 1-s intervals.

The light dependence of assimilation rate was determined in situ on leaves with a portable photosynthesis apparatus (PP systems model CIRAS-1) with the attached illumination unit for the chamber. Leaves were first induced at 600 (*Conostegia*) or 1700 (*Clidemia*) μmol photons m^{-2} s^{-1} and then the light dependence of assimilation was determined by reducing the PFD in steps with neutral density filters. Dark respiration was measured 20 min after darkening the chamber with a black cloth. Photosynthesis rates were determined at ambient temperatures (27–29°C) and CO_2 partial pressures of 380–400 μbar.

Leaf reflectance and transmittance (T) for PFD for each leaf type were measured in an integrating sphere attached to a spectral radiometer (LI-COR model LI-1800). Absorptance was calculated as $1\text{-}r\text{-}T$.

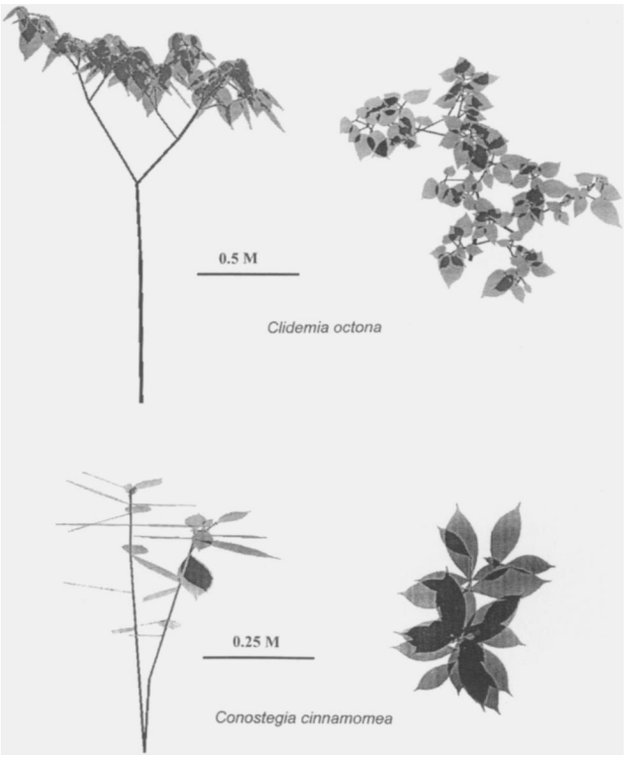

Fig. 2 Images captured from the screen of reconstructed *Conostegia cinnamomea* (*top*) and *Clidemia octona* plants (*bottom*). Images for the solar vectors at 0615 hours and 1215 hours on 9 March are shown on the left and right sides, respectively. The *darkly shaded* areas correspond to areas of leaf overlap and hence self-shading in the model

Results

Computer images generated by YPLANT accurately displayed the arrangement of leaves and stems and the resulting self-shading from any direction (Fig. 2). The view produced by YPLANT is slightly different than that obtained with a camera or with the human eye since it consisted of a parallel projection onto a two-dimensional surface, the monitor screen. The crown of the *Clidemia octona* individual studied mostly consisted of a monolayer with the leaves inclined at 46°±13° (mean ± SD). In contrast, the individual of *Conostegia cinnamomea,* although much smaller in stature and total leaf area, exhibited more of a multilayer crown with the leaves held close to horizontal (leaf angle =13°±10°).

The efficiencies of light capture for diffuse PFD for the two species in their respective light environments differed slightly with values of E_A being 48% and 54% for *Clidemia* and *Conostegia*, respectively. Comparison of E_P and E_D at different elevation angles reveals how leaf angle and self-shading interact in determining the efficiency of a particular crown architecture (Fig. 3). For *Clidemia*, E_P increased only slightly with elevation angle and E_D was only about 10% lower than E_P, indicating relatively little leaf overlap at any elevation angle. The

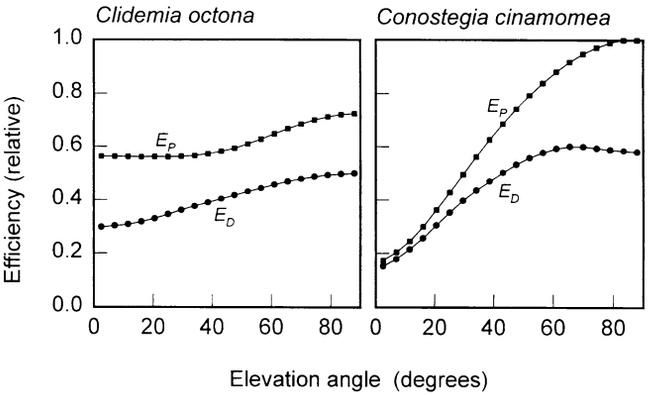

Fig. 3 The dependence of projection efficiency (E_P) and display efficiency (E_d) as a function of elevation angle for the *Clidemia octona* (*left side*) and *Conostegia cinnamomea* (*right side*) plants. Each point is the mean value for all azimuths at that elevation angle

major factors determining the E_A for this species were leaf angles, which influence E_P. Self-shading, which is quantified by the difference between E_P and E_D, had relatively little additional effect on E_A. For *Conostegia*, E_P and E_D depended strongly on elevation angle because of the nearly horizontal leaves in this species. Since the gaps in the overstory canopy were primarily at high ele-

Table 1 List of symbols, units and definitions for the variables used in YPLANT. Variables without units are dimensionless

Symbol	Units	Definition
α	degrees	Elevation angle measured from the horizontal[a]
$\bar{\alpha}$	degrees	Elevation angle to the centroid of a sky sector
A_N	μmol CO_2 m^{-2} s^{-1}	Net photosynthetic rate
A_{MAX}	μmol CO_2 m^{-2} s^{-1}	Light-saturated photosynthetic rate
a		Leaf absorptance
β	degrees	Azimuth[a]
d	mm	Diameter[a]
E_A		PFD absorption efficiency
E_D		Display efficiency
E_P		Projection efficiency
F_{DIF}	μmol photons m^{-2} s^{-1}	Absorbed diffuse PFD
F_{DIR}	μmol photons m^{-2} s^{-1}	Absorbed direct (sunfleck) PFD
F_P	μmol photons m^{-2} s^{-1}	PFD on a plane normal to the solar beam above the overstory
F_M	μmol photons m^{-2} s^{-1}	Solar constant in PFD units
f_{SH}		Fraction of leaf that is shaded
f_{USH}		Fraction of the leaf that is unshaded
G_{SH}		Number of gridpoints within shaded fraction of the leaf
G_{USH}		Number of gridpoints within unshaded fraction of leaf
I_P	μmol photons m^{-2} s^{-1}	Normalized PFD at leaf surface measured normal to the beam
I_{DIF}		Normalized above-canopy diffuse PFD
I_{DIR}		Normalized above-canopy direct PFD
k		Factor reducing sunfleck PFD
L	m^2	Leaf area
L_P	m^2	Projected leaf area
L_D	m^2	Displayed leaf area
LAR	m^2 g^{-1}	Leaf area ratio
LAR_E	m^2 g^{-1}	Effective leaf area ratio
l	mm	Length[a]
M	g	Biomass
P	μmol photons s^{-1}	Absorbed photon flux per gridpoint
R	μmol CO_2 m^{-2} s^{-1}	Dark respiration rate
r		Leaf reflectance
ϕ	mol CO_2 mol^{-1} photons	Quantum yield for CO_2 uptake
θ		Convexity of light response curve
τ_a		Atmospheric transmission coefficient
T		Leaf transmittance
T_C		Canopy transmission coefficient

[a] Subscripts B, L, M, P, S, ST refer to branch, leaf, midrib, petiole, solar and stem, respectively

vation angles (<45°), the reduced E_D at these angles was the primary determinant of E_A in this species. Self-shading was therefore quantitatively more important in *Conostegia* than in *Clidemia*.

Estimates of dry mass showed that the *Clidemia* plant had higher allocation to stems and lower allocation to leaves than the *Conostegia* plant (Table 2). Shoot LAR was 2.5 times greater for the *Conostegia* plant than for the *Clidemia* plant. The LAR_E was 2.4-fold higher for the *Conostegia* than the *Clidemia* plant, largely because of the greater investment in stem biomass in the latter species. Since E_A for the two crowns differed by only about 5% in this instance, the much larger differences in LAR_E were primarily due to the differences in shoot LAR.

Since the functional consequence of crown light capture is whole-plant carbon gain, we included a simple light response curve equation model for simulating photosynthesis. This calculation depends on the simulation of the directional PFD to provide the input so that the leaf by leaf assimilation can be determined. YPLANT was able to simulate diffuse PFD levels on the horizontal plane with an accuracy that depended on the thresholds set for distinguishing gaps in CANOPY and the value of T_E. The measured midday diffuse PFD ranged from 50 to 70 μmol photons m^{-2} s^{-1} for the *Clidemia* site while with a T_E of 0.04, the simulated midday PFD was 90 μmol photons m^{-2} s^{-1}. For the *Conostegia* site, the measured midday diffuse PFD ranged ranged from 8–12 μmol photons m^{-2} s^{-1} while the predict midday PFD with the same T_E was 8.3 μmol photons m^{-2} s^{-1}. Excellent agreement between simulated and measured values of diffuse PFD could be obtained either by adjusting the threshold within CANOPY or the T_E within YPLANT.

Simulation of direct PFD from the canopy photographs alone was less satisfactory, primarily because penumbral effects are not taken into account in the photographic analysis. In addition, there was an approximate but not complete match between the occurrence of a specific sunfleck in the measured records and in the record derived from the solar track on the photo. The simulations for the *Clidemia* site gave reasonable agreement with the measured values but the contribution of sunflecks was greatly overestimated for the *Conostegia* site. Sunflecks at this site typically ranged from 100 to 500 μmol photons m^{-2} s^{-1} because of penumbral effects whereas the sunflecks simulated from the solar track reached full direct-beam PFD (1200–1800 μmol photons m^{-2} s^{-1}) during midday. Changing k from 1 to 0.2 so that

Table 2 Biomass allocation, leaf photosynthetic parameters, and simulated daily light capture and assimilation for *Clidemia octona* and *Conostegia cinnamomea* plants

	Clidemia octona	*Conostegia cinnamomea*
Measurements		
Shoot mass, g	168.0	9.92
Total leaf area, m^2	0.83	0.13
Biomass allocation		
% leaves	21.6	50.3
% petioles	2.2	2.7
% stems	76.2	46.9
Leaf area ratio (shoot only), $m^2\ g^{-1}$	0.0049	0.0127
A_{MAX} (μmol $CO_2\ m^{-2}\ s^{-1}$)	8.3±0.2[a]	6.2±0.01[a]
Respiration rate (μmol $CO_2\ m^{-2}\ s^{-1}$)	0.7±0.01[a]	0.12[b]
Quantum yield (mol $CO_2\ m^{-1}$ photons)	0.045±0.003[a]	0.0552[b]
Leaf absorptance	0.85[b]	0.85[b]
Simulations		
Incident PFD, mol $m^{-2}\ day^{-1}$	18.83	0.44
Absorbed PFD, mol $m^{-2}\ day^{-1}$		
total	9.16	0.23
direct	7.89	0.09
E_A, mol absorbed mol^{-1} incident (diffuse PFD)	0.48	0.54
LAR_E, $m^2\ g^{-1}$	0.0024	0.0069
Daily assimilation, mmol $m^{-2}\ day^{-1}$	108.3	6.6
in direct PFD	56.0	2.8
in diffuse PFD	52.3	3.7

[a] Mean plus standard deviation for measurements on three leaves
[b] Mean for measurements on two leaves

the maximum PFD of the simulated sunflecks was 20% of the direct beam PFD gave good agreement with the measured daily totals with the measured values. As an alternative, we used the sunfleck PFD measurements recorded above each plant to create records of the times of occurrence, the durations and the k values required to give the same integrated PFD in the simulated sunflecks. When this was done for *Conostegia*, YPLANT yielded an estimate of 0.44 mol photons $m^{-2}\ day^{-1}$ with 39% contributed by direct PFD, which was only slightly greater than the actual measurements.

The resulting mean assimilation rates simulated for each plant revealed large differences that were related to the contrasting light environments, canopy structures and photosynthetic capacities of the *Conostegia* and *Clidemia* plants. For the *Clidemia* plant, the daily assimilation was predicted to be 108 mmol $CO_2\ m^{-2}\ day^{-1}$, with 52% of this total contributed by utilization of direct PFD. In contrast, the daily assimilation predicted for the *Conostegia* plant was 6.6 mmol $CO_2\ m^{-2}\ day^{-1}$ with 41% of this total contributed by photosynthesis in direct PFD (sunflecks). In order to examine the role of the architectural differences in the carbon gains we set the leaf physiological parameters of *Clidemia* equal to those of *Conostegia* and then ran simulations for both species using the CANOPY file for the *Conostegia* microsite. Thus the only difference for the two simulations was in crown architecture. Daily carbon gain for *Clidemia* with *Conostegia* leaf physiology and in the *Conostegia* light environment was 5.2 mmol $CO_2\ m^{-2}\ s^{-1}$, or 27% less than simulated for the *Conostegia* plant itself. This simulation indicates that small differences in E_A may have a substantial impact on carbon gain when it is low to begin with because of strongly limiting PFD. The opposite simulation, with both plants having the leaf physiological characteristics of *Clidemia* and in the *Clidemia* light environment revealed much smaller relative differences.

The consequence of the surprisingly large amount of self-shading in the crown of *Conostegia* was examined by using the capability of YPLANT to provide output for individual leaves. When the lowest and uppermost five leaves were compared, the lowest five leaves absorbed a mean daily PFD of 0.162 mol photons $m^{-2}\ day^{-1}$ and had a mean daily assimilation of 3.5 mmol $CO_2\ m^{-2}\ day^{-1}$. In contrast, the upper five leaves, which had no self-shading, absorbed on average 0.419 mol photons $m^{-2}\ day^{-1}$ and had a mean daily assimilation of 15.2 mmol $CO_2\ m^{-2}\ day^{-1}$. This simulation shows that self-shading reduced the mean daily assimilation for the whole *Conostegia* crown by 57%.

Discussion

The model presented here is a considerable advance over previously reported shoot architecture models in its capacity to realistically simulate individual plant crowns from relatively easily implemented field measurements. As shown in the simulations, it is capable of handling a range of plant sizes and architectures and providing a variety of outputs for assessing the consequences of a particular crown morphology. The principal advantages afforded by YPLANT derive from its capacity to reconstruct, in three-dimensional space, a planar image of a crown so that the absorption of radiation incident from

any vector can be determined. Since different physiological or morphological characteristics can be assigned to different leaf classes, it is possible to analyze the consequences for whole plant performance of different resource distributions (e.g. nitrogen) or different physiological capabilities (e.g. sun-shade acclimation) among leaves. Moreover, since YPLANT also outputs information on light capture and assimilation for individual leaves, it is possible to compare the performance of these different leaves as was done for the upper and lower *Conostegia* leaves. The examples given here are images of real canopies, but clearly a "model" crown based on hypothetical leaf orientations, sizes and shapes, and branching patterns, etc. could just as easily be reconstructed for studying how particular morphological characters such as branching patterns (Küppers 1985; Waller and Steingraeber 1986) or combinations of characters influence light capture and carbon gain. The interface with hemispherical canopy photography provides a relatively simple method for determining the magnitude and directional components of incident radiation. Therefore, adaptive responses to particular light environments such as those involving phototropic orientation of leaves can be assessed (see Ackerly and Bazzaz 1995). The simulations in YPLANT also include stems as shade-casting structures, which can be important in some canopies (Miller and Stoner 1979).

Crown architecture models for assessment of light capture fall into two general classes: geometrically based deterministic models such as YPLANT that use either implicitly or explicitly ray tracing techniques to assess light interception, or statistical models in which the probability of light penetration to a particular canopy layer is calculated (see Ross 1981). Early geometric models of individual plants (Honda et al. 1981; Chazdon 1985) were two-dimensional but more recently several three-dimensional models have been reported. The model PHYLO developed by Niklas (1988) is three-dimensional, but is applicable to only relatively simple shoots and simulated only direct light interception. The model of Takenaka (1994), on the other hand, simulates diffuse radiation interception for model shoots with different phyllotaxies and leaf and petiole dimensions. A poplar tree growth model, ECOPHYS (Dickmann et al. 1990), includes a three-dimensional crown model but is species specific. As in YPLANT, each of these models uses a ray tracing approach for determining light interception. A recent model reported by Ryel et al. (1993) for tussock grasses also simulates the three-dimensional architecture of a plant but uses the statistical approach. In the Ryel et al. (1993) model, the tussock is divided into layers and concentric cylinders, with the foliage and stem area specified for each and the interception of radiation calculated from the probabilistic theory of canopy light extinction. The Ryel et al. (1993) model is suited for complex architectures, and larger or denser canopies in which measurements of all individual leaves and stems would be difficult. By contrast, YPLANT is more suited for simulating individual canopies of <200–400 leaves where the ray tracing method would give a more accurate estimate of light interception. While YPLANT could be applied to much larger plants, with a maximum number of nodes limited only by the computer memory available, there is a practical limit set by the measurement effort required.

YPLANT provides several outputs useful in assessment of light capture by a plant, including E_A, E_P and E_D, and when coupled with biomass estimates, LAR_E. Most previous studies have assessed crown light capture performance by estimating either total light capture or E_I values (Chazdon 1985; Niklas 1988; Takenaka 1994). E_A has an advantage over E_I in that it includes the effects of leaf absorptance as well as transmission to shaded leaves. However, since the absorptance of leaves for photosynthetically active radiation is typically high (0.8–0.9) and the fraction transmitted and then absorbed by the intercepting shaded leaf is low, these factors are relatively insignificant as compared to those influencing PFD interception per se. A disadvantage of both E_I and E_A is that they assess the consequences of a particular leaf display of a crown but are leaf area based and therefore do not take into account the biomass costs required to achieve that display. The use of LAR_E overcomes this limitation since it includes both the consequences of the architecture and the biomass allocation costs required to support it. Moreover its close link to LAR, which is known to be a critical determinant of differences in relative growth rates in plants (Lambers and Poorter 1992), may allow it to be an especially useful measure of architectural efficiency for understanding the consequences of differences in crown structure for growth of plants.

The inclusion of a photosynthesis submodel in YPLANT increases its flexibility as an analytical tool for assessment of the relative performances of different crown architectures. Because of the saturation response of photosynthesis, there exists no necessarily linear relationship between the total light intercepted or absorbed and plant performance in terms of carbon gain and growth. Moreover, in high light situations such as gaps, architectures that avoid excess PFD and hence reduce E_A may be advantageous in avoiding photoinhibition. Assessment of how much photosynthesis is reduced by the aviodance strategy at the whole-plant level would be valuable in understanding the costs versus benefits of a particular crown morphology. This simple steady-state model ignores the dynamic responses to sunflecks, which in the understory are could cause as much as a 25% reduction in the carbon gain relative to the steady-state prediction (Pearcy et al. 1994). However, for comparison and assessment of alternative crown architectures, inclusion of only a simple, steady-state light response in YPLANT is probably sufficient for most purposes. Moreover, when photosynthetic light response measurements are not available, YPLANT can still be used, if reasonable guesses, perhaps based on those of ecologically similar species, are made for the photosynthetic parameters. Although more complex photosynthetic models incorporating responses to other environmental factors could be introduced into YPLANT, doing so could reduce its generality

and make it much harder to parameterize. To our knowledge, only two previous crown architecture models (Dickmann et al. 1990; Wang and Jarvis 1990) have been specifically linked to a photosynthesis model.

A limitation inherent in simulating photosynthesis with YPLANT is that, unlike E_A which depends on a ratio of PFDs, prediction of photosynthetic rate depends on the quantitative prediction of PFD from the canopy photographs. Studies of hemispherical canopy photography have revealed high correlations (r^2>0.8) between measured and predicted daily PFD when the comparisons are made over a variety of light environments (Chazdon and Field 1987; Becker et al. 1989). At very low PFDs in the understory, however, the proportional difference between predictions and measurements can be large, principally because of errors associated with prediction of sunflecks. The primary source of error is that penumbral effects are ignored, but for a specific sensor site and day, the match between direct PFD measurements and predictions from a canopy photograph is also influenced by cloud cover, canopy movements in the wind and small errors in camera alignment or negative alignment in the image analysis system (Chazdon and Field 1987). These alignment errors can cause the solar track to miss a particular gap but perhaps hit another. Since A_N exhibits a saturation response, the overestimation of A should be much less than the overestimation of sunfleck PFD caused by ignoring penumbral effects. Therefore, for comparative purposes it may be sufficient to rely on PFD predicted from the canopy photographs. The great advantage in this situation is that only one photograph is needed for predictions at different times during the year. However, if more precise predictions of carbon gain are needed and if direct measurements are available then these can be utilized in place of the sunfleck records derived from the canopy photograph analysis. Also, spot PFD measurements above the plant when sunflecks are absent can be used to adjust either thresholds or T_C to give good matches between the measured and simulated diffuse PFDs.

Although YPLANT was developed primarily with understory plants in mind, it is applicable to a wider range of situations with certain restrictions. It assumes that shading of the crown is by distant objects (i.e an overstory canopy) so that gap geometry as represented by the fisheye photograph holds for all leaves in the crown. This condition will not hold if the shading is primarily cast by a nearby objects such as adjacent plants.

Other assumptions inherent in YPLANT are the result of simplification of complex phenomena, which was necessary for either theoretical or practical reasons. It is assumed that light reflected from a leaf is lost, i.e. that none is intercepted by other leaves in the crown. Similarly, it is assumed that no reflection from the ground back to the plant occurs. Transmitted PFD is also not scattered. Therefore it is assumed that the PFD transmitted through an upper to a lower leaf is independent of distance and that no adjacent leaves receive scattered PFD. In a real crown, these two factors will tend to compensate, so that ignoring scattering is unlikely to introduce a large error. Penumbral effects within the crown are also ignored, which is unlikely to be important for shade plants, given the large leaves and generally short distances between them along the vector of an intercepted beam. However, for small or finely dissected leaves, penumbral effects may become significant for CO_2 assimilation (Oker-Blom 1984).

Comparison of the *Clidemia* and *Conostegia* plants reveals substantial differences in crown structure that in their respective environments lead to relatively small (6%) differences in E_A. Nevertheless, this small difference in E_A was sufficient to cause a 27% difference in simulated daily carbon gain in the understory light environment when all physiological characteristics were set to be identical. Reduction of self-shading within the *Conostegia* crown via longer petioles or internodes or different leaf shapes or sizes could substantially improve the carbon gain. Of course, it remains to be seen if the costs of these changes might offset any benefit. Any crown architecture is a consequence of a large number of shoot and leaf characteristics, and different character combinations may achieve roughly similar efficiencies. The question remains whether this leads to a general convergence in crown light capture efficiencies despite differences in crown morphology, or whether there are unique combinations of characters that indeed provide an advantage is specific situations. The interaction with other factors such as the avoidance of damage due to falling debris, or hydraulic or biomechanical efficiency may also lead to the occurrence of multiple optimal crown architectures (Farnsworth and Niklas 1995). The differences in LAR_E were much more striking, but this may be largely a consequence of the different plant sizes. Ontogenetic drift will generally lead to reduced LAR as plant size increases and may also lead to decreases in light capture efficiency on a leaf area basis (Chazdon 1985; Ackerly and Bazzaz 1995). Thus it is important to compare crowns of similar size, or better yet compare species over a similar range of crown sizes.

Appendix 1

Determination of "stem" geometry in three-dimensional coordinates

We define the "earth" coordinate system as orthogonal coordinates of n (north), e (east) and z (zenith; Fig. 4). Within these coordinates, the orientation of a linear segment, i.e a stem, branch or petiole, can be described by its elevation angle, α, and its azimuth, β.

The vector ($\bar{\mathbf{S}}$) of a stem segment from the nodes at the proximal (p) to the distal (d) end is given by:

$$\bar{\mathbf{S}}.e = \sin\beta \cdot \cos\alpha$$
$$\bar{\mathbf{S}}.n = \cos\beta \cdot \cos\alpha$$
$$\bar{\mathbf{S}}.z = \sin\alpha$$

where β is the azimuth in the direction from p to d and α is the inclination angle from horizontal. If the vector to the proximal end of the stem segment is $\bar{\mathbf{S}}_p$, and the length from p to d is l, then the vector to the distal end ($\bar{\mathbf{S}}_d$) is given by:

$$\bar{\mathbf{S}}_d = \bar{\mathbf{S}}_p + l \cdot \bar{\mathbf{S}}$$

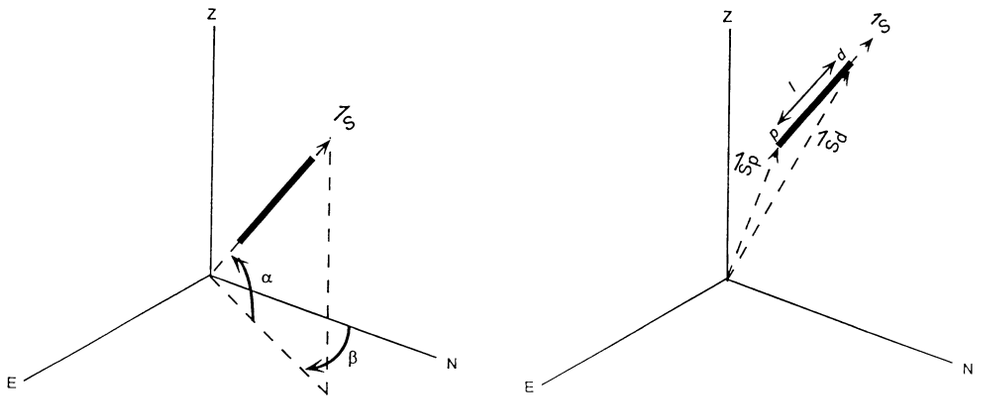

Fig. 4 Diagram showing (*right side*) the definition of a "stem" vector in terms of its angle (α) and azimuth (β) and (*left side*) the definition of the vectors to the proximal ($\bar{\mathbf{S}}_p$) and distal ($\bar{\mathbf{S}}_d$) ends in earth (*E,N,Z*) coordinates

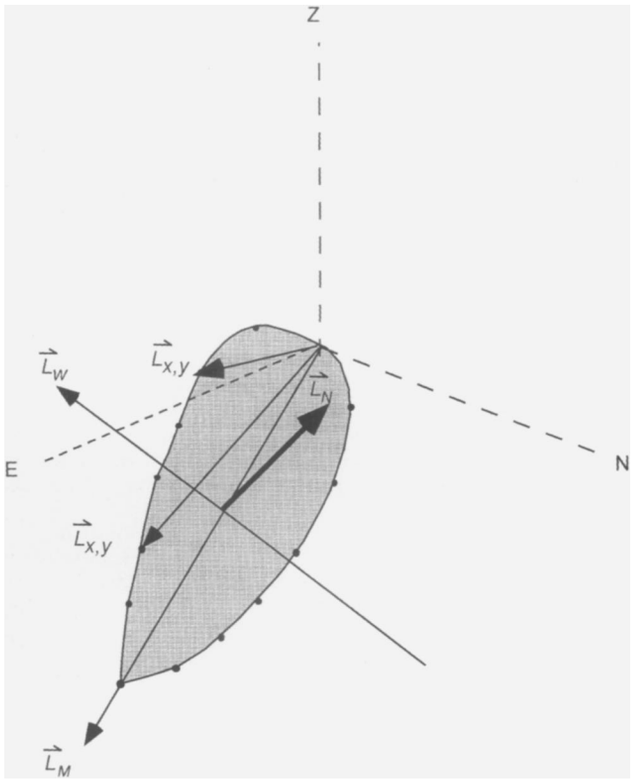

Fig. 5 Diagram showing the method of defining the leaf surface in terms of the *x,y* coordinates for the leaf edge. The vector $\mathbf{L}_N$ is the normal to the leaf surface while $\mathbf{L}_M$ and $\mathbf{L}_W$ are the longitudinal and transverse vectors, respectively. $\mathbf{L}_{x,y}$ are the vectors from the petiole attachment point to the leaf-edge coordinate points

Thus, it follows that

$$\begin{aligned}\bar{\mathbf{S}}_d.e &= \bar{\mathbf{S}}_p.e + l \cdot \bar{\mathbf{S}}.e;\\ \bar{\mathbf{S}}_d.n &= \bar{\mathbf{S}}_p.n + l \cdot \bar{\mathbf{S}}.n;\\ \bar{\mathbf{S}}_d.z &= \bar{\mathbf{S}}_p.z + l \cdot \bar{\mathbf{S}}.z.\end{aligned} \quad (1)$$

Equation set 1 is applied to any linear segment such as a branch or petiole and defines the midpoint of the distal node (or the petiole attachment point). To account for the shade cast by a segment, it is given a diameter (shadow width) equal to the measured diameter.

Determination of the leaf geometry in three-dimensional coordinates

Derivation of the coordinates for the leaf surface follow similar principles, except in this case the two-dimensional nature of the planar surface must be accounted for. The leaf defined in earth coordinates is shown in Fig. 5 where $\bar{\mathbf{L}}_n$ is the vector normal to the leaf surface, $\bar{\mathbf{L}}_w$ is the leaf-length vector, and is the leaf-width vector. Since the coordinates for points along the margin of the leaf outline are based on the leaf-width and leaf-length vectors, it is necessary to first derive $\bar{\mathbf{L}}_w$ and $\bar{\mathbf{L}}_l$ from the measured azimuth and angle of the leaf surface, and the azimuth of the leaf longitudinal axis. Thus,

$$\begin{aligned}\bar{\mathbf{L}}_n.e &= \sin\alpha \cdot \sin\beta\\ \bar{\mathbf{L}}_n.n &= \sin\alpha \cdot \cos\beta\\ \bar{\mathbf{L}}_n.z &= \cos\alpha\end{aligned}$$

and since $\bar{\mathbf{L}}_n$ is perpendicular to $\bar{\mathbf{L}}_l$ and $\bar{\mathbf{L}}_w$, then

$$\begin{aligned}&\bar{\mathbf{L}}_l.e = \sin\omega;\\ &\bar{\mathbf{L}}_l.n = \cos\omega;\\ &\bar{\mathbf{L}}_l.z = -(\bar{\mathbf{L}}_l.e \cdot \bar{\mathbf{L}}_n.e + \bar{\mathbf{L}}_l.n \cdot \bar{\mathbf{L}}_n.n)/\bar{\mathbf{L}}_n.z,\end{aligned}$$

and $\bar{\mathbf{L}}_w = \bar{\mathbf{L}}_l \times \bar{\mathbf{L}}_n$,

it follows that

$$\begin{aligned}\bar{\mathbf{L}}_w.e &= \bar{\mathbf{L}}_l \cdot n.\bar{\mathbf{L}}_n \cdot \mathrm{z} - \bar{\mathbf{L}}_l.z \cdot \bar{\mathbf{L}}_n.n;\\ \bar{\mathbf{L}}_w.n &= \bar{\mathbf{L}}_l \cdot z.\bar{\mathbf{L}}_n \cdot \mathrm{e} - \bar{\mathbf{L}}_l.e \cdot \bar{\mathbf{L}}_n.z;\\ \bar{\mathbf{L}}_w.z &= \bar{\mathbf{L}}_l \cdot e.\bar{\mathbf{L}}_n \cdot \mathrm{n} - \bar{\mathbf{L}}_l.n \cdot \bar{\mathbf{L}}_n.e.\end{aligned}$$

Then, for any leaf edge vector, $\bar{\mathbf{L}}$, with coordinates w_t, l_t(where the subscript indicates the particular leaf type), the vector for the distal end of the petiole, $\bar{\mathbf{P}}_d$, and leaf length, *m*,

$$\begin{aligned}\bar{\mathbf{L}}.e &= (w_t \cdot \bar{\mathbf{L}}_w.e + l_t \cdot \bar{\mathbf{L}}_l.e) \cdot m + \bar{\mathbf{P}}_d.e;\\ \bar{\mathbf{L}}.n &= (w_t \cdot \bar{\mathbf{L}}_w.n + l_t \cdot \bar{\mathbf{L}}_l.n) \cdot m + \bar{\mathbf{P}}_d.n;\\ \bar{\mathbf{L}}.z &= (w_t \cdot \bar{\mathbf{L}}_w.z + l_t \cdot \bar{\mathbf{L}}_l.z) \cdot m + \bar{\mathbf{P}}_d.z.\end{aligned}$$

Appendix 2

Conversion of the three-dimensional architecture from earth to viewpoint coordinates

To determine the interception cross section of the plant, we define a view coordinate system, *x,y,v* with a view plane perpendicular to the light beam and the *V* axis parallel to the beam. For convenience we define the *x* axis as parallel to the earth's surface, and facing to the right, thus creating an image of the plant in the view plane similar to a normal photographic image. If, in earth coordinates, the direction of origin of the light beam is described by its

azimuth, α, and elevation angle, β. The view coordinate vectors, $\bar{\mathbf{X}}$ and $\bar{\mathbf{Y}}$ are given by

$$\bar{\mathbf{X}}.e = -\cos\alpha;$$
$$\bar{\mathbf{X}}.n = \sin\alpha;$$
$$\bar{\mathbf{X}}.z = 0,$$

$$\bar{\mathbf{Y}}.e = -\sin\alpha \cdot \sin\beta;$$
$$\bar{\mathbf{Y}}.n = -\sin\beta \cdot \cos\alpha;$$
$$\bar{\mathbf{Y}}.z = \cos\beta,$$

and since $\bar{\mathbf{V}} = \bar{\mathbf{X}} \times \bar{\mathbf{Y}}$, then

$$\bar{\mathbf{V}}.e = \bar{\mathbf{X}}.n \cdot \bar{\mathbf{Y}}.z - \bar{\mathbf{X}}.z \cdot \bar{\mathbf{Y}}.n;$$
$$\bar{\mathbf{V}}.n = \bar{\mathbf{X}}.z \cdot \bar{\mathbf{Y}}.e - \bar{\mathbf{X}}.e \cdot \bar{\mathbf{Y}}.z;$$
$$\bar{\mathbf{V}}.z = \bar{\mathbf{X}}.e \cdot \bar{\mathbf{Y}}.n - \bar{\mathbf{X}}.n \cdot \bar{\mathbf{Y}}.e.$$

Translation from earth to viewpoint coordinates of any vector then follows

$$\bar{\mathbf{U}}.x = \bar{\mathbf{U}}.e \cdot \bar{\mathbf{X}}.e + \bar{\mathbf{U}}.n \cdot \bar{\mathbf{X}}.n + \bar{\mathbf{U}}.z \cdot \bar{\mathbf{X}}.z;$$
$$\bar{\mathbf{U}}.y = \bar{\mathbf{U}}.e \cdot \bar{\mathbf{Y}}.e + \bar{\mathbf{U}}.n \cdot \bar{\mathbf{Y}}.n + \bar{\mathbf{U}}.z \cdot \bar{\mathbf{Y}}.z;$$
$$\bar{\mathbf{U}}.v = \bar{\mathbf{U}}.e \cdot \bar{\mathbf{V}}.e + \bar{\mathbf{U}}.n \cdot \bar{\mathbf{V}}.n + \bar{\mathbf{U}}.z \cdot \bar{\mathbf{V}}.z;$$

Acknowledgements This research was supported in part by a Smithsonian Institution/Mellon Foundation Senior fellowship to R.W.P. We thank Eloisa Lasso and Suleyka Maynard for their expert assistance with the field work and Fernando Valladares, Robin Chazdon and Yiqi Luo for helpful comments on the manuscript. We also gratefully acknowledge the helpful comments and suggestions from Robin Chazdon and David Ackerly which led to several improvements during the development of YPLANT, and Karl Niklas for providing PHYLO, which in part stimulated development of YPLANT.

References

Ackerly DA, Bazzaz FA (1995) Seedling crown orientation and interception of diffuse radiation in tropical forest gaps. Ecology 76: 1134–1146

Becker P, Erhart DW, Smith AP (1989) Analysis of forest light environments. Computerized estimation of solar radiation from hemispherical canopy photographs. Agric For Meteorol 44: 217–232

Campbell GS (1977) An introduction to environmental biophysics. Springer, Berlin Heidelberg New York, pp 175–177

Chazdon RL (1985) Leaf display, canopy structure and light interception of two understory palm species. Am J Bot 72: 1493–1502

Chazdon RL (1986) The costs of leaf support in understory palms: economy vs. safety. Am Nat 127: 9–30

Chazdon RL, Field CB (1987) Photographic estimation of photosynthetically active radiation: evaluation of a computerized technique. Oecologia 73: 525–527

Dickmann DI, Michael DA, Isebrands JG, Westin S (1990) Effects of leaf display on light interception and apparent photosynthesis in two contrasting *Populus* cultivars during their second growing season. Tree Physiol 7: 7–20

Farnsworth KD, Niklas KJ (1995) Theories of optimization form and function in branching architecture in plants. Funct Ecol 9: 335–363

Fisher JB (1986) Branching patterns and angles in trees. In: Givnish TJ (ed) On the economy of plant form and function. Cambridge University Press, Cambridge, pp 493–524

Fisher JB, Honda H (1977a) Branch geometry and effective leaf area: a study of *Terminalia* branching pattern. I. Theoretical trees. Am J Bot 66: 633–644

Fisher JB, Honda H (1977b) Branch geometry and effective leaf area: a study of *Terminalia* branching pattern. II. Survey of real trees. Am J Bot 66: 645–655

Givnish TJ (1986) Biomechanical constraints on crown geometry in forest herbs. In: Givnish TJ (ed) On the economy of plant form and function. Cambridge University Press, New York, pp 525–584

Gutschick VP, Wiegel FW (1988) Optimizing the canopy photosynthetic rate by patterns of investment in specific leaf mass. Am Nat 132: 67–86

Halle F, Oldemann RAA, Tomlinson PB (1978) Tropical trees and forests: an architectural analysis. Springer, Berlin Heidelberg New York

Honda H, Fisher JB (1978) Tree branch angle: maximizing effective leaf area. Science 199: 888–890

Honda H, Tomlinson PB, Fisher JB (1981) Computer simulation of branch interaction and regulation by unequal flow rates in botanical trees. Am J Bot 68: 569–585

Hutchison BA, Matt DR, McMillen RT (1980) Effects of sky brightness distribution upon penetration of diffuse radiation through canopy gaps in a deciduous forest. Agric For Meteorol 22: 137–147

Kuppers M (1985) Carbon relations and competition between woody species in a Central European hedgerow. IV. Growth form and partitioning. Oecologia 66:343–352

Lambers H, Poorter H (1992) Inherent variation in growth rate between higher plants: a search for physiological causes and ecological consequences. Adv Ecol Res 23: 188–261

Miller PC, Stoner WA (1979) Canopy structure and environmental interactions. In: Solbrig OT, Jain S, Johnson GB, Raven PH (eds) Topics in plant population biology. Columbia University Press, New York, pp 428–458

Monsi M, Uchijima Z, Oikawa T (1973) Structure of foliage canopies and photosynthesis. Annu Rev Ecol Syst 4: 301–328

Myneni RB (1991) Modeling radiative transfer and photosynthesis in three-dimensional vegetation canopies. Agric For Meteorol 55: 323–344

Myneni RB, Impens I (1985) A procedural approach for studying the radiation regime of finite and truncated foliage spaces. II. Experimental results and discussion. Agric For Meteorol 34: 3–16

Niklas KJ (1988) The role of phyllotactic pattern as a "developmental constraint" on the interception of light by leaf surfaces. Evolution 42: 1–16

Oker-Blom P (1984) Penumbral effects of within-plant and between-plant shading on radiation distribution and leaf photosynthesis: a monte-carlo simulation. Photosynthetica 18: 522–528

Pearcy RW, Chazdon RL, Gross LJ, Mott KA (1994) Photosynthetic utilization of sunflecks: A temporally patchy resource on a time scale of to minutes. In: Caldwell MM, Pearcy RW (eds) Exploitation of environmental heterogeneity by plants. Academic Press, San Diego, pp 175–208

Rich PM (1990) Characterizing plant canopies with hemispherical photographs. Remote Sensing Rev 5: 13–29

Ryel RJ, Beyschlag W, Caldwell MM (1993) Foliage orientation and carbon gain in two tussock grasses as assessed with a new whole-plant gas-exchange model. Funct Ecol 7: 115–124

Takenaka A (1994) Effects of leaf blade narrowness and petiole length on the light capture efficiency of a shoot. Ecol Res 9: 109–114

Thornley JHM (1976) Mathematical models in plant physiology. Academic Press, London

Waller DM, Steingraeber D (1986) Branching and modular growth: theoretical models and empirical patterns. In: Jackson JBC, Buss LW, Cook RE (eds) The population biology and evolution of clonal organisms. Yale University Press, New Haven

Wang YP, Jarvis PG (1990) Influence of crown structural properties on PAR absorption, photosynthesis and transpiration in sitka spruce: application of a model (Maestro). Tree Physiol 10: 297–316

Whitehead D, Grace JC, Godfrey MJS (1990) Architectural distribution of foliage in individual *Pinus radiata* D. Don crowns and the effects of clumping on radiation interception. Tree Physiol 7: 135–155